Sensors & Actuators: B. Chemical 458 (2026) 139753

Contents lists available at ScienceDirect

Sensors and Actuators: B. Chemical

journal homepage: www.elsevier.com/locate/snb

Wine discrimination through an electronic nose based on SWCNTs functionalized with Zn phthalocyanine

Sonia Freddi [a,b,*], Monica Bollani [a], Luigi Sangaletti [b]

[a] Institute of Photonics and Nanotechnologies - Consiglio Nazionale delle Ricerche (IFN-CNR), LNESS laboratory, Via Anzani 42, Como 22100, Italy
[b] Surface Science and Spectroscopy Lab at I-Lamp, Department of Mathematics and Physics, Università Cattolica del Sacro Cuore, via della Garzetta 48, Brescia 25133, Italy

ARTICLE INFO

Keywords:
Electronic nose
SWCNTs
Zn phthalocyanine
Wine tracking
Machine learning

ABSTRACT

Ensuring wine quality and authenticity is of growing importance for both producers and consumers, particularly considering the increasing economic relevance of the global wine industry and the need to safeguard consumer trust. Reliable, rapid, and cost-effective tools are required to monitor the progression of wine aging, detect early signs of spoilage, and identify varietal origin, since these parameters are directly linked to both sensory attributes and market value. Here, we report the development of an electronic nose (e-nose) based on single-walled carbon nanotube (SWCNT) sensors functionalized with zinc phthalocyanine (ZnPc), designed to improve sensitivity and selectivity toward wine-related volatile compounds. The e-nose, comprising seven sensors, was characterized using representative analytes such as ethanol, water vapor, ammonia, acetic acid, and acetone, which are key indicators of fermentation, spoilage, and storage conditions. The e-nose was subsequently employed to monitor wine aging and to discriminate among several commercial white wines, including Prosecco, Chardonnay, Pinot Grigio, Lugana, and Prime Rosè. Distinct and reproducible response patterns enabled accurate discrimination of both wine type and aging stage. These results demonstrate the capability of ZnPc-functionalized SWCNT e-nose to provide objective and scalable aroma-based quality evaluation, highlighting its potential for broader applications in the characterization of fermented beverages and complex food matrices.

1. Introduction

Tracking wine quality and authenticity is gaining interest in the global wine industry, for both producer and consumers. Indeed, producers often aim to ensure the quality of their products and exposing potential market frauds, while consumers seek for quality in terms of genuine and not spoiled products. Therefore, on one hand it is important to track the quality of wine in terms of aging, on the other it is mandatory to accurate discriminate among different wine types, tracking origin or type. Indeed, subtle differences in aroma profiles, influenced by factors such as grape variety, fermentation process, storage conditions, and aging, can significantly impact the sensory perception and commercial value of the wine [1,2].

Current methods to track wine quality relies mainly on a combination of sensory evaluation by sommelier and by analytical techniques such as gas chromatography-mass spectrometry (GC-MS), high-performance liquid chromatography (HPLC), or nuclear magnetic resonance (NMR) [3–6]. While these methods offer high sensitivity and specificity, they are often time-consuming, expensive, and require extensive sample preparation and trained technician to properly perform the analysis [6,7]. Furthermore, the subjective nature of sommelier can lead to variability in results. It is clear that there is the need for more objective and reproducible techniques, which should be rapid and low-cost.

Electronic noses (e-noses), i.e. arrays of non-selective gas sensors, have emerged as promising tools for rapid, non-invasive, and real-time monitoring of products in food and beverage industry [8,9]. These arrays are built to mimic the human olfactory system, coupling gas sensors and pattern recognition algorithms to identify complex gas analyte profiles, with application in several fields, like environment, medicine or industry [9–13]. In the framework of wine quality assessment, e-noses can offer several advantages, including high throughput, portability, and the capability to detect changes in aroma associated with both aging and with varietal differences [14,15].

* Corresponding author at: Institute of Photonics and Nanotechnologies - Consiglio Nazionale delle Ricerche (IFN-CNR), LNESS laboratory, Via Anzani 42, Como 22100, Italy.
E-mail address: sonia.freddi@cnr.it (S. Freddi).

https://doi.org/10.1016/j.snb.2026.139753
Received 25 November 2025; Received in revised form 27 January 2026; Accepted 1 March 2026
Available online 6 March 2026

Commercially available electronic noses are predominantly based on metal-oxide semiconductor (MOX) sensors. These devices offer several advantages, such as robustness, relatively low cost, and established manufacturing processes, which have contributed to their widespread adoption. However, MOS-based e-noses also suffer from notable limitations. In particular, they typically require operation at elevated temperatures, leading to increased power consumption and reduced suitability for portable or continuous-monitoring applications. Furthermore, their sensing performance can drift over time, making frequent recalibration necessary to maintain reliability and accuracy [16,17]. These drawbacks limit the scalability and long-term applicability of MOX-based e-noses in fields where low-energy consumption, long-term stability, and minimal maintenance are critical, such as food and beverage quality control. Room for improvements is represented by nanostructured carbon-based materials, such as graphene or carbon nanotubes (CNTs). Thanks to their unique properties (i.e. high surface to volume ratio, exceptional chemical stability and great charge mobility), CNTs have raised interest for disparate applications, including solar cell [18,19], energy storage [20], and gas sensors. In gas sensor field, although being widely exploited as single sensors [21–23], they remain a challenge in the field of electronic noses [10,24,25], especially for application in food and beverage fields [26].

This study explores the development and application of an e-nose based on single walls CNTs (SWCNTs) for detecting wine aging, exploiting a cooking white wine, and discriminating among different types of white wines, including Prosecco, Chardonnay, Pinot Grigio, Lugana, and Prime Rosè. The wines under investigation are commercially available and produced in a precise Italian region: Trentino Alto Adige.

In particular, to improve the sensing capability of SWCNTs, mainly in terms of sensitivity and selectivity, functionalization with metal phthalocyanines, i.e. zinc phthalocyanine (ZnPc), have been performed. It is reported in literature that while CNTs provide a high surface area and excellent electrical conductivity [27,28], ZnPc contributes to target interactions with specific analytes [29]. The combination of these materials in sensor design enables a more accurate detection and discrimination of wine aroma profiles, thereby enhancing quality control and authentication in a cost-effective and scalable manner.

The here developed e-nose, which comprises 7 sensors, is at first tested to selected analytes, such as ethanol, water vapour, ammonia, acetic acid, and acetone, which play a crucial role in assessing wine quality, detecting aging stages, and distinguishing between different types or origins of wines. Indeed, each of these analytes can be consider as marker of specific chemical or microbiological processes that occur during wine production, storage, and aging. In details, ethanol needs to be recognised by the developed e-nose, being the main component, along with water vapour, of wine composition. Additionally, ethanol is the main product of alcoholic fermentation and physical properties of wine are influenced by its concentration [30]. Ammonia is related to nitrogen metabolism during fermentation and microbial activity, especially involving spoilage organisms such as *Brettanomyces* or *Lactobacillus* [31]. High ammonia concentration (above 10 ppm) in wine can denote microbial contamination or protein degradation, which can affect wine aroma and stability [32,33]. Acetic acid is the primary component of volatile acidity in wine and is often associated with spoilage and aging, especially when its concentration exceeds 600–800 ppm [34–36]. Acetone can be a byproduct of microbial metabolism, mainly from bacterial activity. Its presence in wine can be indicative of a not proper storage condition. Acetone concentration in wine can be considered acceptable up to 20 ppm; higher concentration indicates faulty or over-aged wines [37]. Together, monitoring this set of compounds enables a holistic and rapid assessment of wine quality and type using sensor arrays, offering a powerful starting point for non-invasive wine authentication and discrimination. After the preliminary monitoring of these compounds, two experimental investigations were conducted on white wine to further assess the performance of the proposed e-nose. The first experiment focused on the ability of the system to recognize and track wine aging, providing insights into how volatile profiles evolve over time. The second experiment evaluated the capacity of the e-nose to discriminate among different commercially available white wine varieties. Taken together, these tests highlight the robustness of the sensor array in addressing both temporal changes and varietal differences in wine aroma. The obtained results demonstrate a clear and reproducible discrimination capability, confirming the potential of the developed e-nose as an effective tool for objective wine quality assessment and varietal authentication.

2. Experimental

2.1. Sample preparation

The e-nose is composed of 7 chemiresistors based on SWCNTs: one pristine and 6 functionalized with different amount of zinc phthalocyanine (ZnPc) (Fig. 1a-c, Table 1).

Powder of SWCNTs and ZnPc have been purchased from Sigma-Aldrich. Base SWCNTs solution have been prepared by dissolving 1 mg of SWCNTs and 50 mg of sodium dodecyl sulphate (SDS) into 5 ml of MilliQ water and sonicating at room temperature for 1 h (SWCNTs concentration is approximately 0.2 mM). 20 droplets, each of 3 µl volume, have been dropcasted on a 1 × 1 cm^2 plastic foil (for the bare CNTs sample). 6 identical solutions have then been prepared and different amount of ZnPc powder has been added to each vial: 0.5 μg (sample A), 1.0 μg (sample B), 1.4 μg (sample C), 2.4 μg (sample D), 4.0 μg (sample E), and 7.5 μg (sample F), as reported also in Table 1. After 30 min sonication, 20 droplets of each CNTs+ZnPcs solution have been dropcasted on plastic foils (Fig. 1-b). For all samples, the electrical contacts have been made drawing silver paint stripes at the opposite sides of the square foil.

A second batch of samples was prepared using the same CNTs and ZnPc ratios, but dropcasted onto a silicon substrate in order to enable characterization by energy-dispersive X-ray spectroscopy (EDX). The use of silicon was specifically chosen to avoid the charging effects typically observed when employing plastic substrates, thereby ensuring more reliable imaging and compositional analysis.

Finally, two nominally identical sensor arrays were fabricated on plastic substrate, using the same protocol (sensors prepared in pairs for each ZnPc functionalization content). Both batches were characterized electrically, through Raman and EDX spectroscopies, and towards ammonia. Systematic gas and wine sensing experiments were performed on one complete array to ensure internal consistency of the chemometric dataset.

Of note: ZnPc-films fabricated using the same drop-casting volumes employed for CNT/ZnPc hybrids exhibited very high electrical resistance due to the lack of an homogenous conductive network, preventing reliable chemiresistive gas measurements with the present setup, thus they have not been considered in this work.

2.2. Characterization

To characterize the prepared layers energy dispersive X-ray (EDX) spectra have been collected in different areas of the samples. A JEOL (JSM IT800(IS)) system operation at 20 KeV and in planar view has been exploited. To perform quantification, the EDX spectra have been fitted using the SMILE VIEW Jeol software, with the Standardless – ZAF – metal approach. SEM imaging has been performed with a JEOL (JSM IT800(IS)) system working at 3 KeV.

Raman spectra have been acquired on a CGS device with a Renishaw-Invia system (laser excitation at 633 nm) with a 100 × objective. An 1800 lines/mm grating and a laser power of 5 mW have been used for the measurements. Spectra were collected on (i) CNTs film, (ii) ZnPc powder, (iii) the plastic substrate, and (iv) ZnPc-functionalized CNTs films.

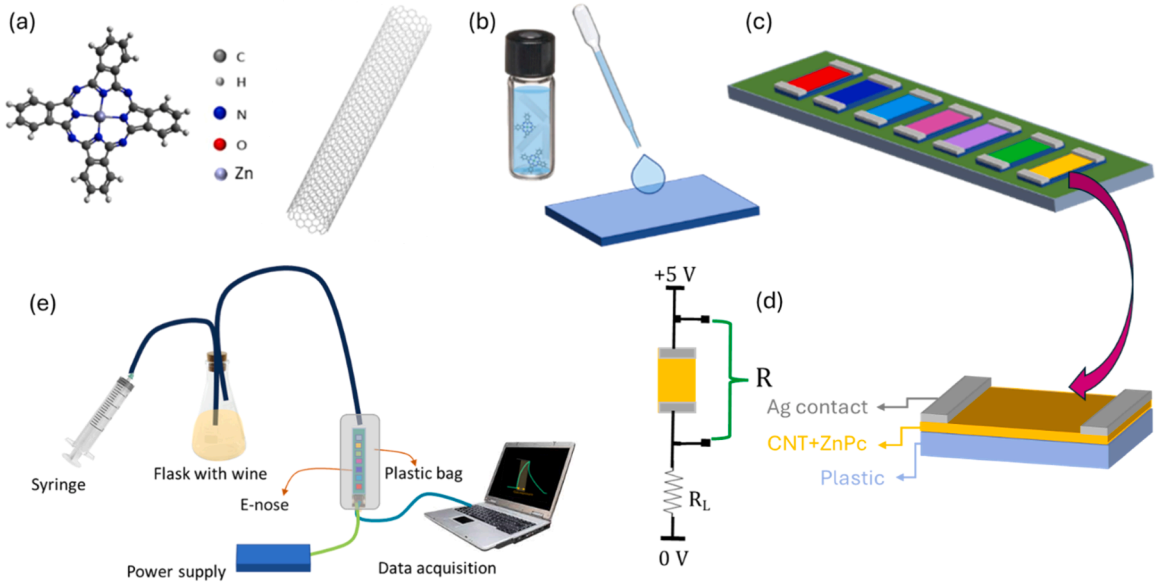

Fig. 1. Summary of the methodology: (a) ZnPc and CNTs powders were weighted and dissolved in different concentration; (b) the solutions were dropcasted on plastic substrates; (c) the prepared samples were then assembled into an electronic nose. (d) cross sectional view of the prepared sensors and readout scheme. (e) Scheme of the set up used to detect wine vapours.

Table 1
summary of the prepared solutions.

Sample Name	CNT (mg) in 5 ml DH_2O	ZnPc (μg)
A	1	0.5
B	1	1.0
C	1	1.4
D	1	2.4
E	1	4.0
F	1	7.5
CNTs	1	-

2.3. Gas and wine sensing measurements

To evaluate the chemoresistive response of the samples to various target gases, electrical contacts were applied using silver paint stripes on opposite sides of each sample. The samples were then mounted on a custom-designed platform, capable of accommodating up to eight sensors, allowing simultaneous monitoring of all sensor responses under the identical environmental conditions (Fig. 1-c).

In addition to the tested sensors, two commercial reference sensors were integrated on the platform: a relative humidity (RH) sensor (Honeywell HIH-4000 series) and a temperature sensor (Murata NTC PCB 5 K thermistor). Data acquisition was managed through a dedicated software written in the LabVIEW environment. Additionally, to monitor the tested gas concentration and draw the calibration curves of the CNTs-based sensors, a properly calibrated commercial sensor that works in parallel to the e-nose has been exploited (FIGARO, TGS2602). Although the TGS2602 is not a strongly selective MOX sensor, it is not used here to claim chemical selectivity, but as a calibrated and reproducible indicator to assign consistent ammonia and ethanol concentrations under controlled temperature, humidity, and background VOC conditions, as also reported in literature [38,39]. The reliability of TGS2602 calibration curves has been cross-checked by measurements in a testing chamber with calibrated mass flow controllers (MFCs) and target analyte cylinders diluted in synthetic air (oxygen 21%, nitrogen 79%) (SIAD S.p.A.), as reported in Figure S1. The MCF connected to the dry air cylinder has a maximum flow of 1000 sccm, while the max flow of the MFC connected to the analyte cylinders is 500 sccm.

Gas-sensing properties were characterized by analysing the chemoresistive response during exposure. Each sensor was connected to a simple electronic readout circuit comprising a load resistor (R_L) in series with the sensor, powered by a constant voltage source (5 V). The sensor resistance (R) was determined by measuring the output voltage across the sensor. The chemoresistive response was then defined and calculated as $\Delta R/R_0 = (R - R_0)/R_0$, where R_0 is the baseline resistance before exposure and ΔR represents the change in resistance during gas exposure. A schematic of this circuit is shown in Fig. 1-d. All CNTs-based sensors worked at an operating temperature of 25°C.

Exposures towards ammonia, acetone, ethanol, acetic acid, and water vapor were performed at room temperature and in laboratory air with a starting relative humidity (RH) of about (50 ± 10)%. Exposure time was set at 3 min, followed by recovery in room air.

In detail, the analytes were produced from a liquid source; indeed, a vial containing few drops of the analyte is placed near the sensors and let evaporate; different concentrations have been achieved changing the liquid volume inside the vial. We consider the starting time of the exposure the instant when the vial is placed near the sensors, while recovery time is defined as the time taken by the sensor signal to recover from its maximum response value to 90% of the total signal change toward the initial baseline after removal of the target gas.

For each exposure, the effective analyte concentration was experimentally determined using the calibrated commercial TGS2602 sensor. All calibration curves are based on the concentration values measured by this reference sensor, not on the nominal liquid volume.

All measurements were performed using the same vial type, opening geometry, sensor-vial distance, and chamber configuration.

For ammonia, which is commonly the gas used to test the performances of new developed sensors, and for ethanol, i.e. the main VOC present in wine, multiple exposures were used to draw the calibration curves by plotting the sensor response ($\Delta R/R_0$) as a function of the gas concentration.

After exposures towards synthetic gas, wine vapours were tested. In detail, wine was inserted into a flask, closed with a cap connected with two small tubes. One of the tubes was connected to a syringe, the other to a plastic bag, where the e-nose was inserted. Air was inserted in the flask through the syringe, to make the wine bubbling. In this way, wine vapours enter the second tube and were sent to the bag containing the e-nose. Wine vapours were left interact with the sensors for about 3 min, then the bag is opened, and the e-nose can recover in fresh air. The set up

for wine test is shown in Fig. 1-e.

All wine measurements were performed under identical experimental conditions to minimize artefacts related to vapor delivery. For each test, bottles were freshly opened, samples were at room temperature, and for each test a new plastic bag was used to avoid carryover or memory effects. Relative humidity and temperature were continuously monitored and remained stable during all wine exposures, while the alcohol content was comparable for all wines (≈10–11% v/v). Sparkling wines (Prosecco and Prime Rosè) were not degassed; they were measured using the same protocol as still wines, and the successful discrimination of all samples will indicate that classification is not dominated by CO_2 release or bubbling-related effects, but by differences in the overall volatile aroma profile.

2.4. Statistical analysis

To evaluate the e-nose capability to discriminate gases, data from exposures to five different analytes were processed using Principal Component Analysis (PCA), whereas for wine aging and wine discrimination, in addition to PCA, Linear Discriminant Analysis (LDA) and Mahalanobis distance calculations were exploited. All chemometric tools were carried out in the R environment.

PCA is an unsupervised chemometric approach used to reduce the dimensionality of a dataset while maintaining the highest variance. It transforms the original variables into a series of orthogonal principal components (PCs), where PC1 captures the largest variance, PC2 the second largest, and so on. The goal is to map the data into a two- or three-dimensional space in which the tested gases can be clearly distinguished [40,41]. LDA, on the other hand, is a supervised chemometric technique that considers class information for each sample. It assumes identical covariance within each class and focuses only on the covariance matrix of the data. Unlike PCA, LDA seeks to maximize the separation between classes while minimizing the spread of data within each class, producing a reduced-dimensional space defined by discriminant factors. This often yields better class separation than PCA, facilitating classification tasks. Additionally, LDA supports both training and testing phases for the dataset [42].

The performance of the LDA-based classification was quantitatively evaluated using accuracy, precision, class recall, and F1-score, computed on the independent test sets. Precision, recall, and F1-score were first calculated for each wine class using a one-versus-rest approach and then summarized using macro-averaging to provide an overall performance metric independent of class size. These metrics allowed a more comprehensive assessment of classification performance beyond overall accuracy, particularly in terms of class-specific discrimination capability.

Finally, Mahalanobis distance was applied within the LDA-transformed space to measure how far a given type of wine lies from the center of each class cluster, providing an alternative method for identifying unknown samples. A Mahalanobis distance of a selected data point is smallest for the class to which it most likely belongs. The algorithm was implemented in R, exploiting the tool in [43].

Before applying PCA, LDA, and Mahalanobis distance analysis, all the three datasets for gas, wine aging and wine classification tests were pre-processed by column mean-centering.

3. Results and discussion

To characterize the samples, several EDX single spectra have been acquired on the 7 prepared layers on silicon substrate (batch1), to avoid charging effects, and representative spectra are shown in Fig. 2-a.

The SDS used for the dispersion of CNTs contributes to the Kα peaks of Na and S, at about 1.1 keV and 2.3 keV, respectively, while the silicon substrate results in the presence of a weak Si Kα peak at 1.7 keV, which intensity is the same in all spectra collected for all samples, indicating that the thickness of the layer is almost the same in all samples. The O Kα peak is detected in all samples, at about 0.5 KeV. C Kα peak is detected at 0.3 keV and it is mainly related to the CNTs layer, while ZnPc contribute to the Zn Lα peak at 1.0 keV.

The aim of EDX analysis is mainly to qualitatively verify a relative C/

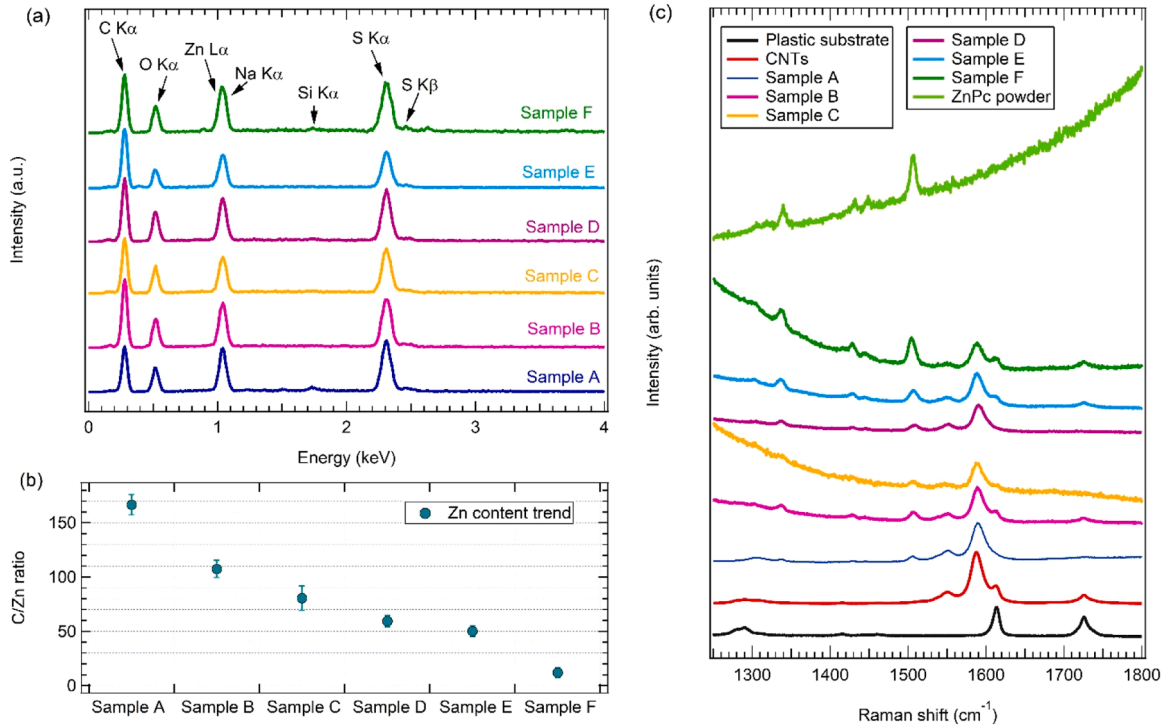

Fig. 2. (a) Representative EDX spectra collected on the functionalized samples. (b) C/Zn ratio as function of the prepared samples. (c) Representative Raman spectra acquired on the plastic substrate (black trace), ZnPc powder (light green trace), bare CNTs (red trace) and on the functionalized samples (blue, pink, yellow, purple, light blue, green traces).

Zn ratio trend. The results, reported in Fig. 2-b, reveal a clear decreasing trend in the C/Zn ratio from Sample A to Sample F, indicating a progressive increase in the ZnPc content relative to the CNTs contribution. The error bars represent the standard deviations obtained upon several measurements in different regions of the samples and demonstrate a good homogeneity of the ZnPc/CNTs intermixing. This systematic reduction in the C/Zn ratio confirms the successful modulation of ZnPc content in the prepared samples.

To assess the chemical composition of the samples, in particular as regard the presence of SDS in the layers, quantification of Na, S and C have been performed from the EDX spectra. In SDS, the theoretical mass ratio of Na:S is 23:32. However, as reported in Table S1, EDX quantification of the prepared samples shows that the Na content is consistently slightly higher than the expected value. This excess of Na can be attributed to trace sodium contamination originating from the water and glassware used during sample preparation. To ensure a reliable evaluation of the SDS content among the samples, the sulfur signal was therefore taken as the reference. Specifically, the C/S ratio was evaluated and found to be nearly identical for all samples, indicating comparable SDS content and making it unlikely that variations in surfactant residue account for the systematic trends observed with ZnPc concentration.

Of note, the overlap between the Na Kα and Zn Lα peaks visible in Fig. 1a was resolved automatically by the JEOL EDX analysis software (SMILE), which deconvolutes overlapping peaks based on reference spectra and fitting algorithms.

Characteristic Raman spectra collected on the prepared samples (batch1), on the plastic substrate and on ZnPc powder are reported in Fig. 2-c. All the spectra have been collected in a 1200–1800 cm^{-1} range, since ZnPcs present a strong luminescence at higher wavenumber [44], which make it difficult to recognize peaks related to CNTs. The CNTs sample (red curve) shows the G-band, with the G^- and G^+ contributions at 1568 cm^{-1} and 1587 cm^{-1}, respectively, and the D-band at 1305 cm^{-1} [45]. The plastic substate contribution (black curve) is mainly related to the peaks at 1280 cm^{-1}, 1610 cm^{-1}, and 1725 cm^{-1}. The main characteristic peaks of ZnPc are located at 1505 cm^{-1}, 1340 cm^{-1}, and 1430 cm^{-1} and 1448 cm^{-1}. For the functionalized samples, contribution from both CNTs and ZnPc can be observed, with a ratio between the two intensities that decreases from Sample A to Sample F, qualitatively confirming once again the increase of the ZnPc content. The ZnPc bands in the composite remain consistent with those of the powder, supporting molecular integrity after processing. Finally, SEM images collected on representative samples (Figure S2) show a similar fibrous and interconnected CNTs network for all functionalized samples. No significant macroscopic morphological changes are observed with increasing ZnPc content, supporting that the functionalization process does not alter the overall CNT structure.

Resistance baseline, Raman and EDX analysis were performed also on the second prepared batch, revealing reproducibility of the preparation protocol (Tables S2, S3 and Figure S3).

Ammonia is considered as the optimal gas to perform preliminary test on sensing capability of nanostructured-carbon-based chemiresistors [46,47]. Thus, we first expose the samples described in Section 2.1 and reported in Table 1, batch1, to ammonia. An example is reported in Fig. 3-a.

To draw the calibration curves, multiple exposures to ammonia at different concentrations, ranging from 0 to 52 ppm, have been performed, and the results are shown in Fig. 4-a. The sensor response is calculated as $\Delta R/R_0$, where R_0 is the baseline resistance before exposure and ΔR represents the change in resistance during gas exposure. A Freundlich isotherm ($\Delta R/R_0 = y + A\cdot[NH_3]^{pow}$) was used to interpolate the data, revealing a sub-linear trend, typical of carbon-based chemiresistors [25,48–50]. The calibration curves clearly indicate that functionalization enhances the sensing response of bare CNTs and that the response increases with the ZnPc content: the lowest response is observed for sample A, followed sequentially by samples B, C, D, E, and F.

Also the recovery time is improved upon functionalization, as can be seen in Fig. 3: indeed, while CNTs sample does not fully recover from ammonia exposure within approximatively 30 min, all the functionalized samples achieved complete recovery, with sample F being the the best-performing also in terms of recovery. It is worth noting that, compared to values reported in the literature [25,51–54], the observed recovery times are consistent, although they remain too long for integration into a continuous food quality monitoring chain, where recovery on the order of a few seconds is typically required [55]. Nevertheless, for wine discrimination purposes, the recovery times achieved are entirely suitable and do not limit the practical application of the device.

To improve recovery times of CNT/ZnPc chemiresistors to meet industrial level requirements, several strategies can be considered. Thermal or UV-assisted desorption can accelerate the release of adsorbed volatile compounds from the sensor surface, while mild airflow or pulsed heating can help restore baseline resistance more rapidly [56–58]. These strategies can be explored in future works.

To assess the batch-to-batch reproducibility, 4 prepared samples were selected and tested in pairs towards ammonia, in order to evaluate variations between the two different batches. Only four sensors per batch were considered, as the platform can host up to eight sensors. The selected sensors were CNTs, and samples A, C, and F, to test different ZnPc concentration. The results, reported in Figure S4, demonstrate comparable sensor responses across batches, within the experimental measurement uncertainty (below 5%).

In addition to ammonia, calibration curves have been drawn also for ethanol exposures, in a 0–105 ppm range, being ethanol the main VOC present in wine (Figs. 3-b and 4-b), considering only samples from batch1. As in the case of ammonia exposures, also for ethanol tests an increase of the resistance is observed, and it is also clear that better performances in terms of response and recovery time are observed for the functionalized samples. In particular, CNTs sample shows a very week response towards ethanol, almost in the noise, which is clearly enhanced and with a positive trend within the increase of ZnPc concentration in the functionalized samples. A sublinear behaviour of the response vs concentration is observed also in the case of ethanol, and Freundlich isotherm has been selected to fit the calibration curves.

The detection limit (dl), i.e. the lowest concentration that the sensor can detect, was evaluated through the formula $5\sigma/R_0 = y + A\,[dl]^{pow}$ [39,59], where σ is the fluctuation of the electrical signal, and A, y and pow are the fitting parameters obtained from the Freundlich isotherm (Fig. 4) and reported in Table S4. The evaluated dl are reported in Table S4. As can be seen, for ammonia the dl is always in the ppb range, while in the case of ethanol Samples C, D, E and F exhibit a dl in the ppb regime, while CNTs, Samples A and B present a dl of some tens of ppm. In both cases, the dl is in general lower for the functionalized sensors compared to the CNTs one. The obtained dl are in line or even better to similar CNT- and carbon-based chemiresistors, especially for ammonia detection [44,50,59–64].

Regarding the sensing mechanism, the observed increase of the resistance value upon exposure to ammonia suggests that all layers exhibit an overall p-type character, which is consistent with the p-type nature of the CNTs-based layers. SWCNTs detect ammonia mainly through charge-transfer due to Van der Waals interactions between the gas molecule and the nanotube surface. Indeed, when the N atom of ammonia molecules faces the surface of SWCNTs, they transfer electrons to the nanotube surface [64,65]. Since pristine SWCNTs generally exhibit p-type semiconducting behaviour [66,67], due to oxygen adsorption from air, this electron donation leads to a partial neutralization of the majority hole carriers, resulting in a decrease in the hole concentration. Consequently, the electrical resistance of the SWCNT network increases. Regarding the functionalized samples, let us consider at first the situation in air. Under ambient conditions without target gases, an electron charge transfer occurs between CNTs and ZnPc, slightly modifying the carrier concentration in the nanotube network

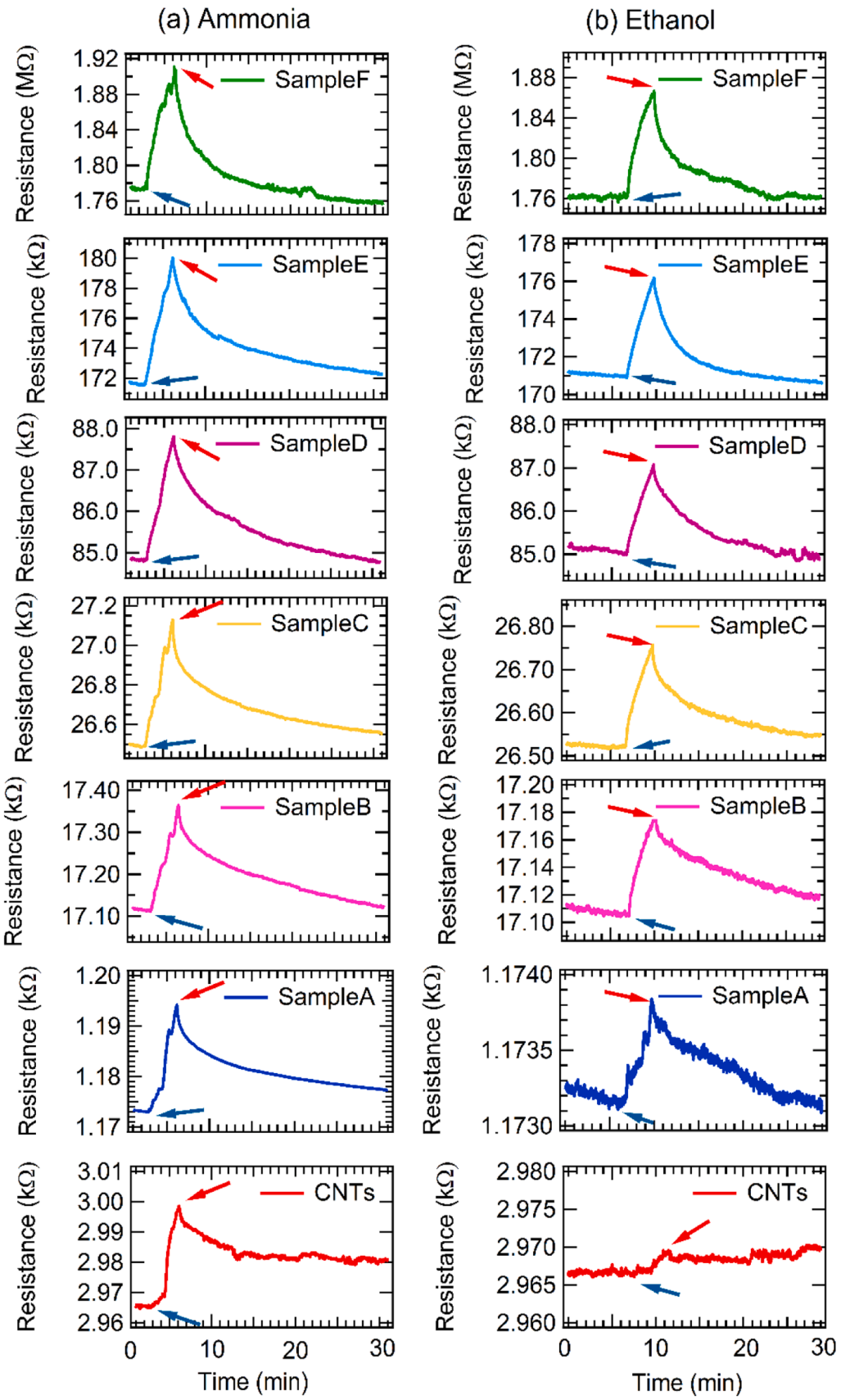

Fig. 3. dynamical response curve, i.e. resistance vs. time for the 7 sensors composing the e-nose during exposure to (a) 52 ppm of ammonia, and (b) 90 ppm of ethanol. Blue arrows indicate the starting points of the exposure, red arrows indicate the end point of the exposure. Sensors worked at room temperature.

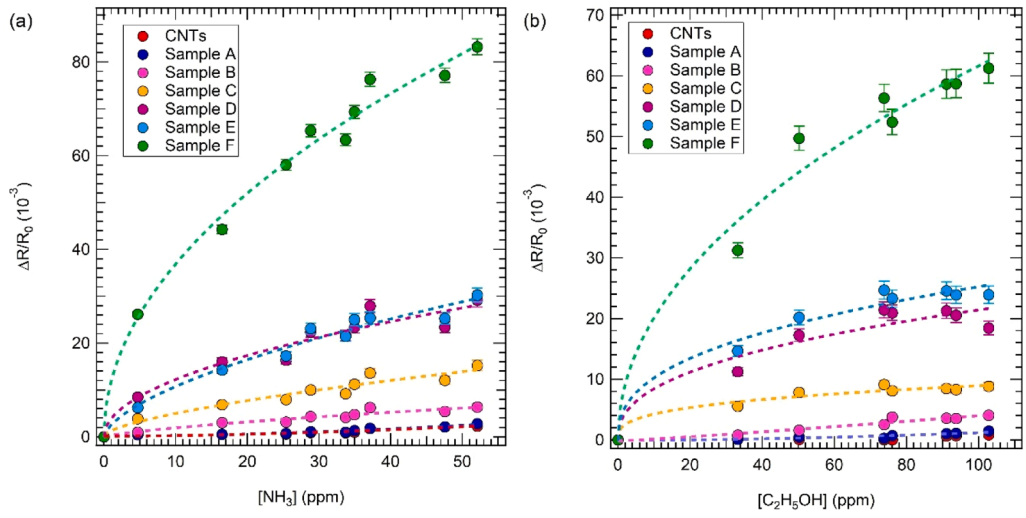

Fig. 4. calibration curves for (a) ammonia and (b) ethanol, evaluated for all the sensors in the e-nose and acquired at room temperature. Dashed lines represent the Freundlich isotherm fit.

[68–71]. It is worth to notice that we observed a gradual increase of the baseline resistance upon functionalization (Fig. 3), from about 2.9 kΩ of the CNTs sample to about 1.8 MΩ of sample F, suggesting that the charge is transferred from the ZnPc molecules to the CNTs network. In particular, it is important to further comment on the progressive increase in baseline resistance observed with increasing ZnPc functionalization, which is attributed to electronic effects rather than to a loss of network percolation. Indeed, SEM images confirm that all samples retain a continuous and interconnected CNTs network. At the microscopic level, ZnPc molecules can modify CNT-CNT junctions and induce charge-transfer interactions, locally increasing tunnelling barriers and modulating carrier density without disrupting macroscopic electrical connectivity. Consequently, the resistance variation reflects intrinsic electronic modulation of the CNT network rather than morphological degradation or percolation artifacts.

Let us consider the sensing mechanism upon exposure to ammonia, when the gas molecules donate electrons to the CNTs but also to the ZnPc, either through interaction with the macrocyclic π-system or, more efficiently, with coordination to the central Zn^{2+} ion, which increases electron density in ZnPc [69,72,73]. This additional electron population is partially transferred to the CNTs, reducing the hole concentration and leading to the measurable increase in the resistance value. The experimentally observed correlation between ZnPc content and ammonia response is consistent with this sensing mechanism: indeed, increasing the ZnPc concentration, there is an increase in the number of active sites available for the charge-transfer interactions, i.e. a higher number of Zn^{2+} ions.

As for ethanol exposures, considering pristine CNTs, the sensing mechanism is mainly governed by weak charge-transfer interactions. Ethanol molecules, possessing a polar hydroxyl group, can act as mild electron donors via their oxygen lone pairs or influence the local dielectric environment upon physisorption [74,75]. This electron donation decreases hole concentration in CNTs, resulting in an increase in electrical resistance. When CNTs are functionalized with ZnPc, the sensing mechanism is influenced by the additional interaction pathways provided by the phthalocyanine molecules. Ethanol can interact with ZnPc through hydrogen bonding between its hydroxyl group and the macrocyclic nitrogen atoms, as well as through weak donor–acceptor interactions with the π-conjugated system [76]. These interactions can modulate the electronic structure of ZnPc and facilitate charge transfer to the CNTs, amplifying the sensing response.

To summarize, previous studies have demonstrated that ZnPc acts as a preferential adsorption site for different classes of gas molecules: electron-donating species such as ammonia interact strongly with the central Zn^{2+} ion through coordination [69,72,73], whereas polar VOCs such as ethanol preferentially interact with the π-conjugated macrocycle via donor-acceptor and hydrogen-bonding interactions [77]. In both cases, ZnPc effectively concentrates the analyte at the sensor surface, enhancing charge-transfer to the underlying carbon nanotube network.

Finally, long-term stability and reproducibility of the sensor response have been proven for ammonia as a representative analyte. As shown in Figure S5, sensor responses recorded up to 4 months after fabrication remain consistent with the calibration trends within experimental uncertainty, indicating no significant degradation over this period. Even after 12 months from the sensors preparation, the response towards ammonia is still reasonably stable, showing a signal loss of below 5%.

Datasets similar to those reported for ammonia and ethanol in Fig. 3 have been collected for exposures to acetone, acetic acid and water, with the aim of probing the discrimination capability of the array. Histograms reported in Fig. 5 have the purpose to show the responses of the e-nose to the 5 selected target molecules expressed as the sensor response $\Delta R/R_0$, evaluated for the highest concentration tested of each analyte. All the sensors respond to all the tested analytes, and the functionalization always enhance the response.

A 8 × 41 response matrix has been used to perform chemometric analysis, being 41 the exposures performed at different concentrations of the 5 tested gases, and 8 the sensors composing the e-nose. Indeed, in addition to the 7 CNTs-based sensors, also the response from the commercial RH (relative humidity) sensor has been added to the matrix. Indeed, water vapor, represented as relative humidity, is recognized as one of the main interfering gases affecting a sensor performance. Peng et al. demonstrated that varying RH levels can significantly impact data clustering when analysed using PCA [78]. We have previously implemented a method to properly consider this aspect: adding the RH sensor response directly into the PCA data matrix can improve the separation of different gases within the PCA space [25,61].

The PCA results are reported in Fig. 6. In the spaces defined by PC1 and PC2 (Fig. 6-a) and by PC1 and PC3 (Fig. 6-b), distinct separation among all tested gas molecules is achieved. Additionally, consistent with previous findings on arrays based on carbon nanomaterials [79], each gas cluster displays a clear concentration gradient, where concentration levels diminish progressively along PC1, from the right to the left. The loading plots (Fig. 6-c) can provide additional insights on the contribution of each sensor toward the gas molecules discrimination. All the sensors, except RH, basically equally contribute to the discrimination along PC1, while the main responsible of discrimination along PC2 are

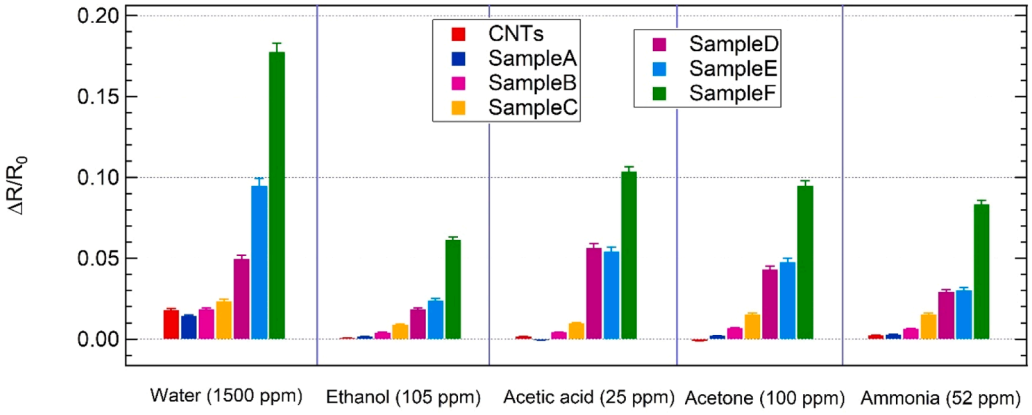

Fig. 5. Histograms with the response $\Delta R/R_0$ of the e-nose to the 5 analytes under investigation for the highest concentration tested. All exposures are performed with the sensors operating at room temperature.

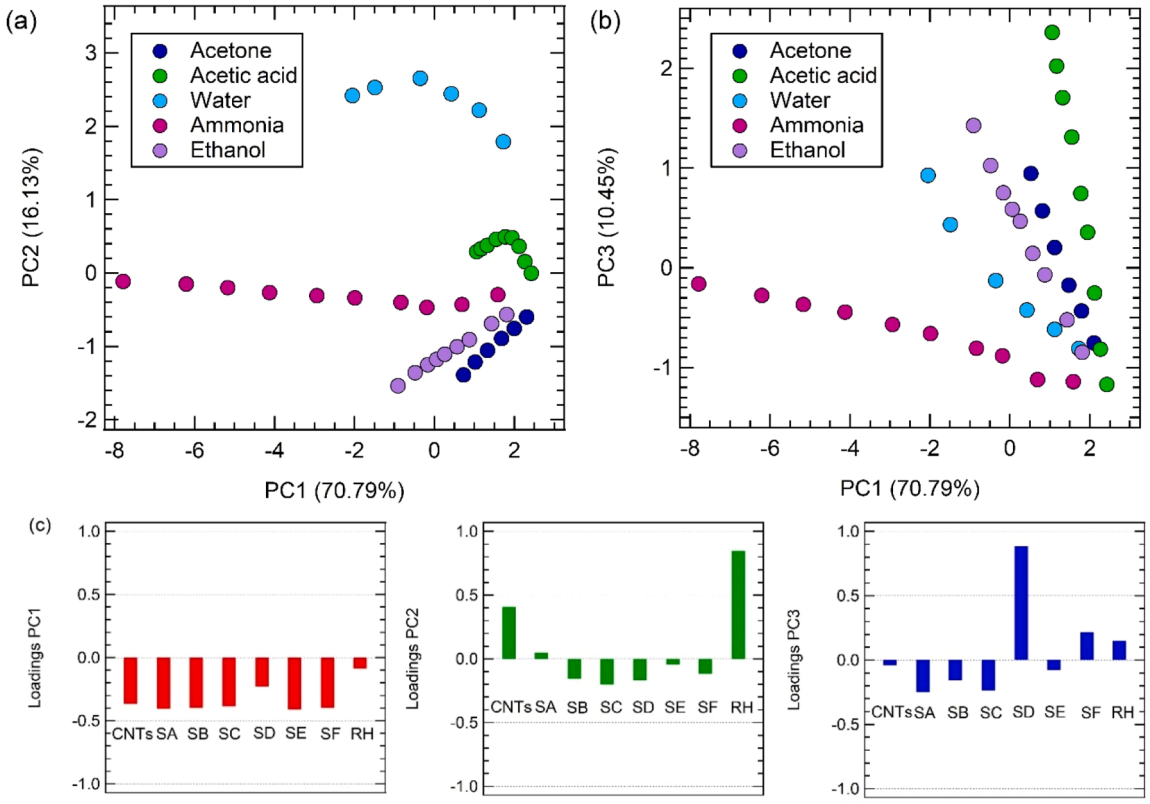

Fig. 6. PCA of the e-nose responses to exposure to ammonia, water, acetone, ethanol and acetic acid concentrations: (a) PC2 vs PC1 and (b) PC3 vs PC1 (c) Loadings for PC1, PC2 and PC3. For clarity, 'S' in the loading caption stands for 'sample', while RH stands for 'RH sensor'.

RH and CNTs sensors, which interestingly are negatively correlated to all the other sensors, and sample D dominates PC3 discrimination. From the loadings we can clearly conclude that all the sensors are necessary to achieve such discrimination.

It is worth noting that the sensing strategy adopted in this work does not rely on highly selective single sensors, but rather on an array of partially cross-sensitive elements whose combined responses are interpreted through multivariate analysis. While individual sensors respond to multiple analytes, the overall response patterns enable clear discrimination at the system level, as demonstrated by the PCA separation of five wine-related volatile compounds (Fig. 6). This array-level selectivity is further validated by the successful discrimination of real wine vapors, which are intrinsically complex mixtures of VOCs, indicating that cross-sensitivity is effectively handled by the chemometric approach.

Additionally, regarding the selectivity, the e-nose was intentionally designed to target key wine-related compounds associated with aging and spoilage, such as ethanol, ammonia, acetic acid, acetone, and water vapor. Other aroma constituents commonly present in wine, including esters and terpenes, were not individually tested. However, their interaction with ZnPc-functionalized CNTs is expected to be weaker due to their lower polarity and reduced charge-transfer capability compared to the selected target analytes [80,81].

Once the capability of the e-nose to discriminate the tested analytes, which are related to wine and wine aging, has been assessed, exposures to wine vapours have been performed. At first a generic white wine for

cooking has been used and its spoilage has been tracked. PCA has been performed on an 8 × 26 data matrix and the results, reported in Fig. 7-a, display the discrimination of cooking white wine samples at three different stages: freshly opened (blue circles), after three weeks of opening (orange squares), and expired one year prior the opening (red triangles). Notably, the clusters corresponding to each condition are well separated along PC1, with the expired samples positioned on the far left, the three-weeks opened samples in the centre, and the freshly opened samples on the right. This clear distinction highlights the progressive chemical changes in the wine detectable by the e-nose over time. The green arrow indicates the trend of sample aging or degradation. It is worth noting also the spread of the single data points inside each cluster: for the freshly opened wine, the e-nose is able to track the differences from bottle to bottle, indicating sensitivity to subtle compositional differences even among samples of the same type. In contrast, the 3-weeks opened and expired wine clusters show more compact groupings, suggesting that aging or degradation of the products cancelled the difference among the different bottles.

Regarding the loadings, sample F exhibits the strongest positive loading along PC1. Interestingly, sample F is the sensor that in general exhibit the highest response towards all the gases identified as markers of wine aging. Regarding PC2, all sensors contribute positively with similar magnitudes, except for the RH sensor, which shows a negative loading. This suggests that PC2 may capture variance potentially linked to subtle changes in the sensor array response to chemical constituents in the wine.

Overall, the data demonstrate that the e-nose, particularly when considering the combined responses weighted by PCA, effectively differentiates cooking white wine samples based on storage time and freshness.

Finally, 6 different wine types have been tested, namely Chardonnay, Lugana, Pinot grigio, Prime Rosè, Prosecco and the cooking white wine. All the wine present similar alcohol percentage, i.e. about 10–11%. A 8 × 49 data matrix has been used and the PCA results are reported in Fig. 8.

The PCA score plots show clear separation among the six wine types, with PC1 explaining 69.11% of the total variance and PC2 and PC3 accounting for 14.88% and 10.56%, respectively. The distinct, non-overlapping clusters indicate that the e-nose effectively discriminates between wine varieties. The loading plots reveal that for PC1, CNTs and Sample A contribute positively while the remaining sensors contribute negatively, suggesting complementary sensing behaviour. PC2 loadings are relatively balanced across sensors, whereas PC3 is dominated by a strong positive contribution from Sample D. These results highlight the combined role of multiple sensing elements in enhancing classification performance.

In particular, for both gas and wine experiments, considering the loadings (Figs. 6c, 7b,d and 8c), no single sensor dominates the PCs responsible for class separation; instead, discrimination arises from the complementary responses of the full sensor array. This indicates that reducing the number of sensors would likely decrease the information content and compromise classification performance. The RH sensor also plays an active role beyond interference monitoring, contributing significantly to higher-order PCs by capturing humidity-related variance intrinsically associated with wine vapours, thereby improving the robustness of multivariate discrimination.

Additionally, it is worth pointing out that, as mentioned in Section 2.3, although sparkling wines (Prosecco and Prime Rosè) were not degassed and they were measured using the same protocol as still wines, the successful discrimination of all samples clearly indicate that classification is not dominated by CO_2 release or bubbling-related effects, but by differences in the overall volatile aroma profile.

PCA is an unsupervised chemometric tool that does not allow for probability of classification, making it unsuitable for direct performance quantification. On the contrary, LDA allows for a predictive and quantitative analysis. LDA uses a training dataset to determine the optimal linear combination of sensor outputs, maximizing inter-class separation while minimizing intra-class variability. Once trained, the model can project test data into the discriminant space, enabling identification of previously unknown samples. To this purpose, the 49 data collected from the 6 wines have been divided into 2 subsets for training and testing; different ratio between training and testing data will be tested. Internal cross validation (CV) of the model has been assessed with CV segment equal to 6: building the model, the LDA algorithm randomly removes 6 datapoints and uses these data to test the newly built model, providing an accuracy of the model itself. In Fig. 9 the LDA space obtained from a training dataset that contains 35 data point is reported. Considering this LDA model, the test dataset composed by of 15 unidentified data has been used to validate the model. The model has been able to recognize and correctly assign each point to the correct class, achieving a prediction accuracy of 100%.

To further probe the LDA capability, several different combinations of training-test datasets dimension (i.e., 49–0, 35–14, 30–19, 27–22, 25–24, 23–26 and 20–29), have been considered and the obtained accuracy of internal validation and prediction are reported in Fig. 9-b. The cross-validation accuracy ranges from 100% to 97.5%, while prediction accuracy goes from 100% to 98%.

The performance of the LDA-based classification was quantitatively evaluated using accuracy, precision, class recall, and F1-score, computed on the independent test sets. In particular, these parameters are constant to 1 for the 49–0, 35–14, 30–19, 27–22 training-test datasets, since the accuracy is 100%. We thus report precision, class recall,

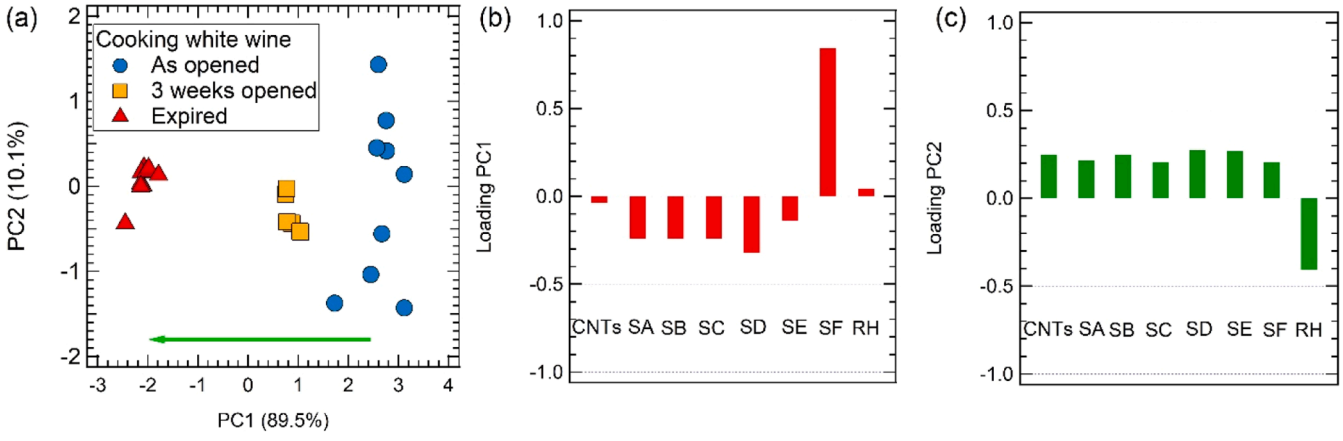

Fig. 7. PCA of the e-nose responses to a cooking white wine at different stages, as opened, after 3 weeks from opening, and expired 1 year prior opening: (a) PC2 vs PC1, (b) Loadings for PC1, (c) Loading for PC2.

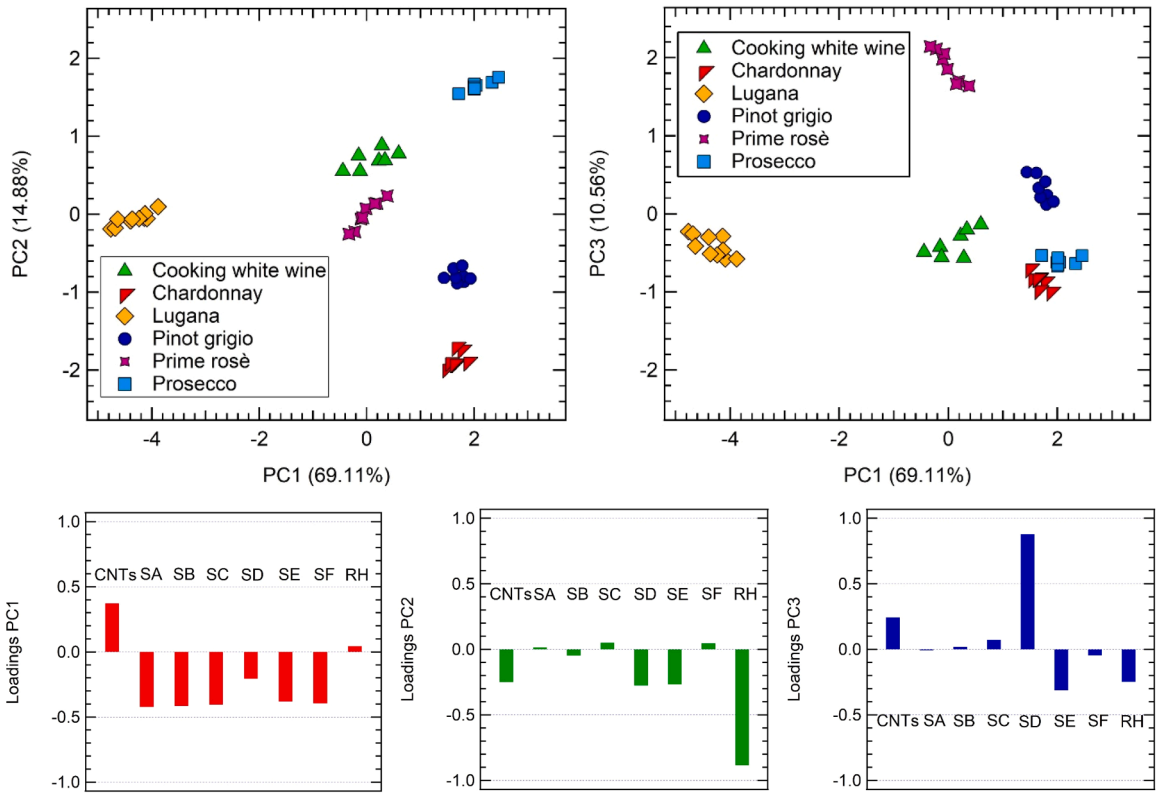

Fig. 8. PCA of the e-nose responses to 6 different white wines: (a) PC2 vs PC1, (b) PC3 vs PC1, (c) Loadings for PC1, PC2 and PC3.

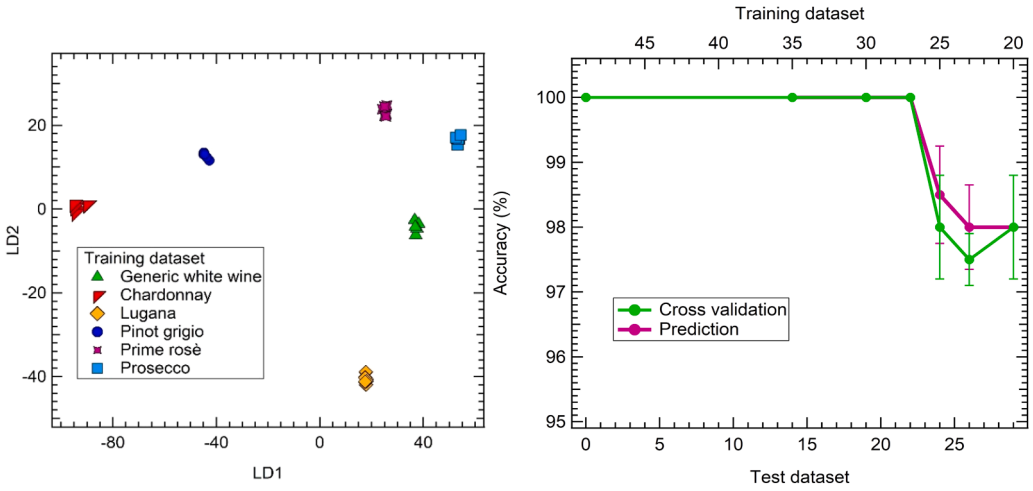

Fig. 9. (a) Example of an LDA space obtained considering a training dataset containing 34 exposures towards the 6 tested wines. (b) Accuracy percentage as function of the training-test datasets dimension for internal cross validation (green dots) and prediction (purple dots). Bottom axis: test dataset dimension (N, with $0 < N < 29$). Top axis: training dataset dimension (49-N).

and F1-score for the 25–24, 23–26 and 20–29 training-test datasets, considering the worst-case scenario for each sub-set. The representative confusion matrices are reported in Tables S5, S7, S9 and S11, whereas the evaluated precision, class recall, and F1-score for each class are reported in Table S6, S8, S10 and S12. The mean precision values are 0.97, 0.94, 0.94, and 0.94; average class recall 0.93, 0.92, 0.93 and 0.93, whereas the Macro-F1 score is 0.96, 0.92, 0.93 and 0.92. These results represent the lowest limit and demonstrate that, even in the worst performances cases, the Macro-F1-score mean class recall and mean precision support the consistency of the analysis and the trustfulness of the results.

Finally, after external validation it is possible to investigate the distance of each point in the test dataset from the different gas clusters, generated by the LDA model, and recognize the belonging class as function of the distance: the smallest distance identifies the class which the point belongs to. To carry out this task, Mahalanobis distance algorithm, being the most exploited for classification, has been considered in the case of the model reported in Fig. 9, and an example of the obtained results are reported in Fig. 10.

In this particular example, it is clear that point 1 belongs to the Prime Rosè, point 2 to Pinot, point 3 is a Lugana, point 4 is the cooking white wine, point 5 is the Chardonnay and point 6 is a Prosecco.

The Mahalanobis distance analysis provides a complementary, distribution-based interpretation of the LDA results. While accuracy,

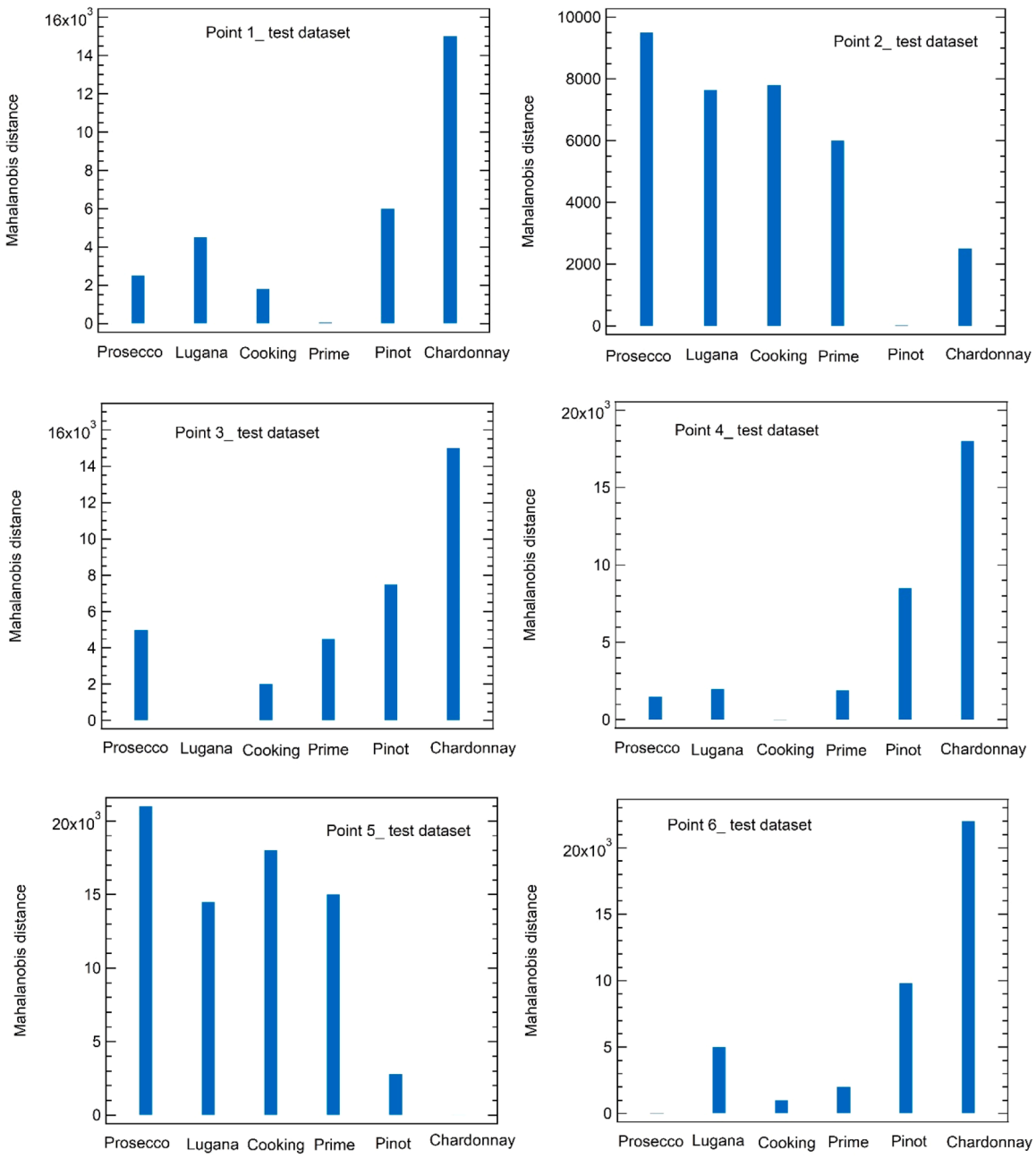

Fig. 10. Mahalanobis distance evaluated by way of example for six points of the test dataset containing 15 data. Of note: 'cooking' stands for 'cooking white wine', while 'Prime' stands for 'Prime Rosè'.

precision, recall, and F1-score quantify the classification performance, the Mahalanobis distance directly measures the statistical separation between class distributions in the feature space, taking into account their covariance. Large inter-class Mahalanobis distances indicate limited overlap between class clusters and, consequently, a reduced probability of misclassification. This behaviour is fully consistent with the high precision and recall values and with the low level of confusion observed in the corresponding confusion matrices (Table S5-S12).

The present results then support the application potential for this e-nose, even with a relatively small dataset, such as the one reported in this study. While PCA performs remarkably well in the discrimination of each gas contribution, for a practical application where prediction is required with a specific accuracy, LDA should be preferred.

4. Conclusion

This work demonstrates the successful development and application of a SWCNT-based e-nose functionalized with ZnPc for wine quality monitoring and discrimination. At first, the enhancement of sensing parameters, including response, selectivity and recovery time, thanks to the ZnPc functionalization has been assessed, as well as the discrimination capability of the e-nose towards wine-related volatile compounds, including ethanol, ammonia, acetic acid, acetone, and water vapour. A clear correlation between ZnPc content and sensing performance has been found, justified considering the sensing mechanism.

Wine has then been tested; at first to follow the evolution of aging and spoilage of a generic cooking white wine, and then to probe the discrimination capability of the e-nose towards 6 different wine variety. Chemometric analysis confirmed the e-nose robust discrimination

capability in both tests. In detail, the e-nose successfully tracked wine aging stages in a PCA 2D-space, detecting chemical profile changes between freshly opened, partially aged, and expired samples. PCA enabled also a clear separation of the different tested wines, while LDA and Malhanobis distance provided quantitative classification with remarkable prediction accuracy in distinguishing between the six commercial wines.

In this study, the analysis was intentionally restricted to commercially available white wines from the same region and with comparable alcohol content, to reduce confounding variables and assess the intrinsic discrimination capability of the e-nose under controlled conditions. Despite this conservative scenario, clear separation among wine types and aging stages was achieved, indicating high sensitivity to subtle differences in volatile composition. Wines from different regions, red wines, or samples with varying alcohol content are expected to exhibit even more pronounced differences in aroma profiles and sensor responses and will be the subject of future investigations aimed at extending the generality of the proposed approach.

Compared with existing e-nose technologies applied to wine analysis, our CNT/ZnPc chemiresistor array presents complementary advantages. For example, compared to the MOX-based e-noses [82,83] or resistive microheater arrays [84] used to discriminate wines, the proposed CNT/ZnPc array operates at room temperature without the need for heaters, offering lower power consumption and simpler hardware compared to most MOX systems that require elevated operating temperatures.

Additionally, the functionalization tunability of CNTs with varying ZnPc concentrations allows tailored sensitivity and cross-sensitivity profiles, which can enhance discrimination of chemically subtle differences. This flexible design is less accessible in traditional MOX arrays.

Finally, it is worth to mention that the demonstrated long term stability under laboratory ambient conditions suggests that the sensors can maintain reliable performance over extended periods, a key requirement for industrial applications. The intrinsic chemical robustness of SWCNTs and metal phthalocyanines, combined with room-temperature operation, minimizes degradation from thermal and chemical stress. These properties indicate that the sensor array is well-suited for practical deployment in industrial environments, where long-term reliability and reproducibility are critical.

In summary, these findings highlight the potential of CNT–ZnPc e-nose as compact, rapid, and low-cost tool for objective wine quality control and authentication. While the current study focused on white wines from a specific region, the methodology is readily extendable to other varietals, production areas, and beverage sectors.

CRediT authorship contribution statement

Sonia Freddi: Writing – original draft, Visualization, Validation, Software, Methodology, Investigation, Funding acquisition, Formal analysis, Data curation, Conceptualization, Writing - review & editing. **Monica Bollani:** Writing – review & editing, Resources, Funding acquisition. **Luigi Sangaletti:** Writing – review & editing, Supervision, Resources, Conceptualization, Funding acquisition.

Declaration of Competing Interest

The authors declare that they have no known competing financial interests or personal relationships that could have appeared to influence the work reported in this paper.

Thus, the authors declare no competing interests.

Acknowledgments

S.F. acknowledges 5 × 1000 fund 2023 allocated at Università Cattolica for partial financial support and Fondazione Cariplo, within BREATH-SENSE 2023–1506. M.B. acknowledges “AGRITECH” project (Centro Nazionale per le Tecnologie dell’Agricoltura, Finanziato dall’Unione Europea – Next Generation EU-PNRR 2022–25).

Appendix A. Supporting information

Supplementary data associated with this article can be found in the online version at doi:10.1016/j.snb.2026.139753.

Data availability

Data will be made available on request.

References

[1] R. Ascrizzi, Y. Pieracci, B. Melai, P.L. Cioni, P. Narri, G. Flamini, L. Pistelli, Preliminary study on red wine aroma: the volatile profiles of six grape cultivars in different vinification phases, Fermentation 8 (12) (2022) 753, https://doi.org/10.3390/fermentation8120753.
[2] D. Zhang, Z. Wei, Y. Han, Y. Duan, B. Shi, W. Ma, A review on wine flavour profiles altered by bottle aging, Molecules 28 (18) (2023) 6522, https://doi.org/10.3390/molecules28186522.
[3] J.E. Welke, K.C. Hernandes, K.P. Nicolli, J.A. Barbará, A.C.T. Biasoto, C.A. Zini, Role of gas chromatography and olfactometry to understand the wine aroma: achievements denoted by multidimensional analysis, J. Sep. Sci. 44 (1) (2021) 135–168, https://doi.org/10.1002/jssc.202000813.
[4] P. Zhang, M. Piergiovanni, P. Franceschi, F. Mattivi, U. Vrhovsek, S. Carlin, Application of comprehensive 2D gas chromatography coupled with mass spectrometry in beer and wine VOC analysis, Analytica 4 (3) (2023) 347–373, https://doi.org/10.3390/analytica4030026.
[5] Z.A. Temerdashev, A.G. Abakumov, O.N. Shelud’ko, Y.F. Yakuba, T.G. Tsyupko, Chromatographic methods in the identification and determination of the component composition and quality of wines, J. Anal. Chem. 79 (10) (2024) 1364–1386, https://doi.org/10.1134/S1061934824700734.
[6] P.A. Solovyev, C. Fauhl-Hassek, J. Riedl, S. Esslinger, L. Bontempo, F. Camin, F. NMR spectroscopy in wine authentication: an official control perspective, Compr. Rev. Food Sci. Food Saf. 20 (2) (2021) 2040–2062, https://doi.org/10.1111/1541-4337.12700.
[7] J. Guasch, O. Busto, Wine: gas and liquid chromatography. Encyclopedia of separation science, Elsevier, 2020, pp. 4490–4498, https://doi.org/10.1016/B0-12-226770-2/01181-9.
[8] M. Wang, Y. Chen, Electronic nose and its application in the food industry: a review, Eur. Food Res. Technol. 250 (1) (2024) 21–67, https://doi.org/10.1007/s00217-023-04381-z.
[9] M. Roy, B.K. Yadav, Electronic nose for detection of food adulteration: a review, J. Food Sci. Technol. (2022) 1–13, https://doi.org/10.1007/s13197-021-05057-w.
[10] S. Freddi, L. Sangaletti, Trends in the development of electronic noses based on carbon nanotubes chemiresistors for breathomics, Nanomaterials 12 (17) (2022) 2992, https://doi.org/10.3390/nano12172992.
[11] F. Furizal, A. Ma'arif, A.A. Firdaus, W. Rahmaniar, Future potential of E-nose technology: a review, Int. J. Robot. Control Syst. 3 (3) (2023) 449–469, https://doi.org/10.31763/ijrcs.v3i3.1091.
[12] S. He, J. Wen, B. Cao, G. Shi, M. Zhang, Porous material-based electronic noses for the sensing of volatile organic compounds, ACS Appl. Mater. & Interfaces 17 (44) (2025) 60055–60103, https://doi.org/10.1021/acsami.5c17506.
[13] H. Guo, T. Liu, X. Zhai, Z. Qu, Y. Zhang, J. Wen, S. Xue, J. Li, J. Tang, T.-P. Huynh, M.G. Li, G. Shi, M. Zhang, Hierarchical porous aggregate-enabled chromatography-inspired single-sensor E-nose for volatile monitoring, ACS Sens. 10 (2) (2025) 1334–1345, https://doi.org/10.1021/acssensors.4c03231.
[14] G. Alfieri, M. Modesti, R. Riggi, A. Bellincontro, Recent advances and future perspectives in the E-nose technologies addressed to the wine industry, Sensors 24 (7) (2024) 2293, https://doi.org/10.3390/s24072293.
[15] M. Aleixandre, J.P. Santos, I. Sayago, J.M. Cabellos, T. Arroyo, M.C. Horrillo, A wireless and portable electronic nose to differentiate musts of different ripeness degree and grape varieties, Sensors 15 (4) (2015) 8429–8443, https://doi.org/10.3390/s150408429.
[16] A.D. Wilson, M. Baietto, Applications and advances in electronic-nose technologies, Sensors 9 (7) (2009) 5099–5148, https://doi.org/10.3390/s90705099.
[17] D. Zappa, V. Galstyan, N. Kaur, H.M.M. Arachchige, O. Sisman, E. Comini, Metal oxide-based heterostructures for gas sensors: A review, Anal. Chim. Acta 1039 (2018) 1–23, https://doi.org/10.1016/j.aca.2018.09.020.
[18] S. Freddi, S. Achilli, R. Soave, S. Pagliara, G. Drera, A. De Poli, F. De Nicola, M. De Crescenzi, P. Castrucci, L. Sangaletti, Dramatic efficiency boost of single-walled carbon nanotube-silicon hybrid solar cells through exposure to ppm nitrogen dioxide in air: an ab-initio assessment of the measured device performances, J. Colloid Interface Sci. 566 (2020) 60–68, https://doi.org/10.1016/j.jcis.2020.01.038.
[19] M. K. A. Mohammed, A.K. Al-Mousoi, S. Singh, A. Kumar, M.K. Hossain, S.Q. Salih, P. Sasikumar, R. Pandey, A. A. Yadav, Z.Mundher Yaseen, Improving the performance of perovskite solar cells with carbon nanotubes as a hole transport layer, Opt. Mater. 138 (2023) 113702, https://doi.org/10.1016/j.optmat.2023.113702.

[20] Z. Han, D. Du, F. Zhang, CNTs composite aerogel incorporating phase-change microcapsules for solar-thermal conversion and energy storage, Carbon 237 (2025) 120125, https://doi.org/10.1016/j.carbon.2025.120125.
[21] G. Verma, A. Gupta, Recent development in carbon nanotubes based gas sensors, Mater. Nanosci. 9 (1) (2022) 3–12. ⟨https://pubs.thesciencein.org/journal/index.php/jmns/article/view/282/231⟩.
[22] S.M. Aalam, M. Sarvar, M. Sadiq, J. Ali, A highly sensitive surface-modified porous carbon nanotube-based sensor for ammonia gas detection, ACS Omega 9 (4) (2024) 4486–4496, https://doi.org/10.1021/acsomega.3c07244.
[23] S.Y. Guo, P.X. Hou, F. Zhang, C. Liu, H.M. Cheng, Gas sensors based on single-wall carbon nanotubes, Molecules 27 (17) (2022) 5381, https://doi.org/10.3390/molecules27175381.
[24] P. Dariyal, S. Sharma, G.S. Chauhan, B.P. Singh, S.R. Dhakate, Recent trends in gas sensing via carbon nanomaterials: outlook and challenges, Nanoscale Adv. 3 (23) (2021) 6514–6544, https://doi.org/10.1039/D1NA00707F.
[25] S. Freddi, G. Drera, S. Pagliara, A. Goldoni, L. Sangaletti, Enhanced selectivity of target gas molecules through a minimal array of gas sensors based on nanoparticle-decorated SWCNTs, Analyst 144 (13) (2019) 4100–4110, https://doi.org/10.1039/C9AN00551J.
[26] T. Zhang, Y. Cao, M. Chen, L. Xie, Recent advances in CNTs-based sensors for detecting the quality and safety of food and agro-product, J. Food Meas. Charact. 17 (3) (2023) 3061–3075, https://doi.org/10.1007/s11694-023-01850-7.
[27] M. Ouyang, J.L. Huang, C.M. Lieber, Fundamental electronic properties and applications of single-walled carbon nanotubes, Acc. Chem. Res. 35 (12) (2002) 1018–1025, https://doi.org/10.1021/ar0101685.
[28] I.V. Zaporotskova, N.P. Boroznina, Y.N. Parkhomenko, L.V. Kozhitov, Carbon nanotubes: sensor properties. a review, Mod. Electron. Mater. 2 (4) (2016) 95–105, https://doi.org/10.1016/j.moem.2017.02.002.
[29] S. Freddi, C. Marzuoli, G. Drera, S. Pagliara, L. Sangaletti, Targeting biomarkers in the gas phase through a chemoresistive electronic nose based on graphene functionalized with metal phthalocyanines, RSC Adv. 13 (1) (2023) 251–263, https://doi.org/10.1039/D2RA07607A.
[30] D. Wollan, D.T. Pham, K.L. Wilkinson, Changes in wine ethanol content due to evaporation from wine glasses and implications for sensory analysis, J. Agric. Food Chem. 64 (40) (2016) 7569–7575, https://doi.org/10.1021/acs.jafc.6b02691.
[31] A. Gobert, R. Tourdot-Maréchal, C. Sparrow, C. Morge, H. Alexandre, Influence of nitrogen status in wine alcoholic fermentation, Food Microbiol. 83 (2019) 71–85, https://doi.org/10.1016/j.fm.2019.04.008.
[32] J. Badura, M. Medić, N.V. Wyk, B. Krause, H. Semmler, S. Brezina, I.S. Pretorius, D. Rauhut, C.V. Wallbrunn, Synthesis of aroma compounds as a function of different nitrogen sources in fermentations using non-Saccharomyces wine yeasts, Microorganisms 11 (1) (2022) 14, https://doi.org/10.3390/microorganisms11010014.
[33] J. Sanz, S. de Marcos, O. Muro, J. Galbán, Ammonium determination in wine by gas phase molecular absorption spectrometry, Microchim. Acta 110 (1993) 193–204, https://doi.org/10.1007/BF01245104.
[34] M.M. Macías, A.G. Manso, C.J.G. Orellana, H.M.G. Velasco, R.G. Caballero, J.P. C. Chamizo, Acetic acid detection threshold in synthetic wine samples of a portable electronic nose, Sensors 13 (1) (2012) 208–220, https://doi.org/10.3390/s130100208.
[35] A. Mas, M.J. Torija, M.D.C. García-Parrilla, A.M. Troncoso, Acetic acid bacteria and the production and quality of wine vinegar, Sci. World J. 2014 (1) (2014) 394671, https://doi.org/10.1155/2014/394671.
[36] D. Zgardan, I. Mitina, R. Sturza, V. Mitin, S. Rubtov, C. Grajdieru, E. Behta, F. Inci, N. Haciosmanoglu, A survey on acetic acid bacteria levels and volatile acidity in several wines of the Republic of Moldova, Biology and Life Sciences, Forum 26 (1) (2023) 79, https://doi.org/10.3390/Foods2023-15153.
[37] H. Hopfer, J. Nelson, S.E. Ebeler, H. Heymann, Correlating wine quality indicators to chemical and sensory measurements, Molecules 20 (5) (2015) 8453–8483, https://doi.org/10.3390/molecules20058453.
[38] F. Rigoni, G. Drera, S. Pagliara, A. Goldoni, L. Sangaletti, High sensitivity, moisture selective, ammonia gas sensors based on single-walled carbon nanotubes functionalized with indium tin oxide nanoparticles, Carbon 80 (2014) 356–363, https://doi.org/10.1016/j.carbon.2014.08.074.
[39] S. Freddi, D. Perilli, L. Vaghi, M. Monti, A. Papagni, C. Di Valentin, L. Sangaletti, Pushing down the limit of NH_3 detection of graphene-based chemiresistive sensors through functionalization by thermally activated tetrazoles dimerization, ACS nano 16 (7) (2022) 10456–10469, https://doi.org/10.1021/acsnano.2c01095.
[40] R. Bro, A.K. Smilde, Principal component analysis, Anal. Methods 6 (2014) 2812, https://doi.org/10.1039/C3AY41907J.
[41] C.B.Y. Cordella, PCA: the basic building block of chemometrics, Anal. Chem. 47 (2012), https://doi.org/10.5772/51429.
[42] P. Reimann, A. Schütze, Sensor arrays, virtual multisensors, data fusion, and gas sensor data evaluation. Gas Sensing Funda-mentals, Springer, Berlin, Heidelberg, 2013, pp. 67–107, https://doi.org/10.1007/5346_2013_52.
[43] R. Leardi, C. Melzi, G. Polotti, CAT (Chemometric Agile Tool), freely downloadable from ⟨http://gruppochemiometria.it/in-dex.php/software⟩.
[44] S. Freddi, L. Vaghi, A. Penoni, L. Scapinello, L. Sangaletti, A minimal electronic nose based on graphene functionalized with metalated pyrazinoporphyrazines and phthalocyanines for ammonia, benzene, and hydrogen sulfide discrimination, Chemosensors 13 (5) (2025) 165, https://doi.org/10.3390/chemosensors13050165.
[45] M.S. Dresselhaus, G. Dresselhaus, R. Saito, A. Jorio, Raman spectroscopy of carbon nanotubes, Phys. Rep. 409 (2005) 47–99, https://doi.org/10.1016/j.physrep.2004.10.006.
[46] A. Casotto, G. Drera, D. Perilli, S. Freddi, S. Pagliara, M. Zanotti, L. Schio, A. Verdini, L. Floreano, C. Di Valentin, L. Sangaletti, π-Orbital mediated charge transfer channels in a monolayer Gr–NiPc heterointerface unveiled by soft X-ray electron spectroscopies and DFT calculations, Nanoscale 14 (36) (2022) 13166–13177, https://doi.org/10.1039/D2NR02647C.
[47] D. Perilli, S. Freddi, M. Zanotti, G. Drera, A. Casotto, S. Pagliara, L. Schio, L. Sangaletti, C. di Valentin, Design of highly responsive chemiresistor-based sensors by interfacing NiPc with graphene, Commun. Mater. 5 (1) (2024) 254, https://doi.org/10.1038/s43246-024-00693-z.
[48] H. Song, X. Li, P. Cui, S. Guo, W. Liu, X. Wang, Morphology optimization of CVD graphene decorated with Ag nanoparticles as ammonia sensor, Sens. Actuators B 244 (2017) 124–130, https://doi.org/10.1016/j.snb.2016.12.133.
[49] N.S. Struchkov, A.V. Romashkin, M.K. Rabchinskii, S.D. Saveliev, P. D. Cherviakova, R.G. Chumakov, A.V. Emelianov, Aminated reduced graphene oxide-carbon nanotube composite gas sensors for ammonia recognition, Sens. Actuators B 417 (2024) 136088, https://doi.org/10.1016/j.snb.2024.136088.
[50] S. Freddi, P. Carro, A.H. Creus, L. Sangaletti, M.C. Rodriguez Gonzalez, Selective enhancement of graphene ammonia sensing by electrochemical palladium nanoparticle decoration: ab initio insights into the sensing response, Nanoscale 17 (2025) 25187–25198, https://doi.org/10.1039/D5NR02547H.
[51] M.N. Norizan, N.S. Zulaikha, A.B. Norhana, M.I. Syakir, A. Norli, Carbon nanotubes-based sensor for ammonia gas detection–an overview, Polimery 66 (3) (2021) 175–186, https://doi.org/10.14314/polimery.2021.3.3.
[52] A. Nijkoops, M. Ciocca, S. Krik, A. Douaki, A. Gurusekaran, S. Vasquez, S, M. Petrelli, M.A. Costa Angeli, L. Petti, P. Lugli, Flexible and printed chemiresistive ammonia gas sensors based on carbon nanotube and conjugated polymers: a comparison of response and recovery performance, IEEE Sens. Lett. 7 (6) (2023) 1–4, https://doi.org/10.1109/LSENS.2023.3274909.
[53] F. Rigoni, S. Freddi, S. Pagliara, G. Drera, L. Sangaletti, J.M. Suisse, M. Bouvet, A. M. Malovichko, A.V. Emelianov, I.I. Bobrinetskiy, Humidity-enhanced sub-ppm sensitivity to ammonia of covalently functionalized single-wall carbon nanotube bundle layers, Nanotechnology 28 (25) (2017) 255502, https://doi.org/10.1088/1361-6528/aa6da7.
[54] F. Rigoni, S. Tognolini, P. Borghetti, G. Drera, S. Pagliara, A. Goldoni, L. Sangaletti, Enhancing the sensitivity of chemiresistor gas sensors based on pristine carbon nanotubes to detect low-ppb ammonia concentrations in the environment, Analyst 138 (24) (2013) 7392–7399, https://doi.org/10.1039/C3AN01209C.
[55] M. Galvani, S. Freddi, L. Sangaletti, Disclosing fast detection opportunities with nanostructured chemiresistor gas sensors based on metal oxides, carbon, and transition metal dichalcogenides, Sensors 24 (2) (2024), https://doi.org/10.3390/s24020584.
[56] K. Drozdowska, A. Rehman, A. Krajewska, D.V. Lioubtchenko, K. Pavłov, S. Rumyantsev, J. Smulko, G. Cywiński, Effects of UV light irradiation on fluctuation enhanced gas sensing by carbon nanotube networks, Sens. Actuators B Chem. 352 (2022) 131069, https://doi.org/10.1016/j.snb.2021.131069.
[57] I. Ahmad, D. Lee, M. Chae, H.D. Kim, Advanced recovery and enhanced humidity tolerance of CNTs gas sensor using a filament heater, Chem. Eng. J. 496 (2024) 154014, https://doi.org/10.1016/j.cej.2024.154014.
[58] D. Kumar, P. Tandon, P.K. Chaudhury, P. Chaturvedi, A. Chouksey, Investigation of single wall nanotube gas sensor recovery behavior in the presence of UV, Adv. Mater. Lett. 7 (4) (2016) 262–266, https://doi.org/10.5185/amlett.2016.5938.
[59] S. Freddi, M. Vergari, S. Pagliara, L. Sangaletti, A chemiresistor sensor array based on graphene nanostructures: from the detection of ammonia and possible interfering VOCs to chemometric analysis, Sensors 23 (2) (2023) 882, https://doi.org/10.3390/s23020882.
[60] L.A. Panes-Ruiz, M. Shaygan, Y. Fu, Y. Liu, V. Khavrus, S. Oswald, T. Gemming, L. Baraban, V. Bezugly, G. Cuniberti, Toward highly sensitive and energy efficient ammonia gas detection with modified single-walled carbon nanotubes at room temperature, ACS Sens. 3 (1) (2018) 79–86, https://doi.org/10.1021/acssensors.7b00358.
[61] S. Freddi, A.V. Emelianov, I.I. Bobrinetskiy, G. Drera, S. Pagliara, D.S. Kopylova, M. Chiesa, G. Santini, N. Mores, U. Moscato, A.G. Nasibulin, P. Montuschi, L. Sangaletti, Development of a sensing array for human breath analysis based on SWCNT layers functionalized with semiconductor organic molecules, Adv. Healthc. Mater. 9 (12) (2020) 2000377, https://doi.org/10.1002/adhm.202000377.
[62] A.G. Bannov, M.V. Popov, A.E. Brester, P.B. Kurmashov, Recent advances in ammonia gas sensors based on carbon nanomaterials, Micromachines 12 (2) (2021) 186, https://doi.org/10.3390/mi12020186.
[63] S. Brahim, S. Colbern, R. Gump, A. Moser, L. Grigorian, Carbon nanotube-based ethanol sensors, Nanotechnology 20 (23) (2009) 235502, https://doi.org/10.1088/0957-4484/20/23/235502.
[64] D. Maity, K. Rajavel, R.T.R. Kumar, Polyvinyl alcohol wrapped multiwall carbon nanotube (MWCNTs) network on fabrics for wearable room temperature ethanol sensor, Sens Actuators B Chem. 261 (2018) 297–306, https://doi.org/10.1016/j.snb.2018.01.152.
[65] K.Y. Dong, J. Choi, Y.D. Lee, B.H. Kang, Y.Y. Yu, H.H. Choi, B.K. Ju, Detection of a CO and NH_3 gas mixture using carboxylic acid-functionalized single-walled carbon nanotubes, Nanoscale Res. Lett. 8 (1) (2013) 12, https://doi.org/10.1186/1556-276X-8-12.
[66] R. Tang, Y. Shi, Z. Hou, L. Wei, Carbon nanotube-based chemiresistive sensors, Sensors 17 (4) (2017) 882, https://doi.org/10.3390/s17040882.
[67] P.G. Collins, K. Bradley, M. Ishigami, D.A. Zettl, Extreme oxygen sensitivity of electronic properties of carbon nanotubes, Science 287 (5459) (2000) 1801–1804, https://doi.org/10.1126/science.287.5459.1801.
[68] L.M. Arellano, L. Martín-Gomis, H.B. Gobeze, D. Molina, C. Hermosa, M.J. Gómez-Escalonilla, J.L.G. Fierro, A. Sastre-Santos, F. D'Souza, F. Langa, Edge-on and face-

on functionalized Pc on enriched semiconducting SWCNT hybrids, Nanoscale 10 (11) (2018) 5205–5213, https://doi.org/10.1039/C8NR00262B.
[69] P. Krasnov, V. Ivanova, D. Klyamer, A. Fedorov, T. Basova, Phthalocyanine-Carbon Nanotube Hybrid Materials: Mechanism of Sensor Response to Ammonia from Quantum-Chemical Point of View, Chemosensors 10 (11) (2022) 479, https://doi.org/10.3390/chemosensors10110479.
[70] P.O. Krasnov, T.V. Basova, A. Hassan, Interaction of metal phthalocyanines with carbon zigzag and armchair nanotubes with different diameters, Appl. Surf. Sci. 457 (2018) 235–240, https://doi.org/10.1016/j.apsusc.2018.06.282.
[71] E.V. Basiuk, L. Huerta, V.A. Basiuk, Noncovalent bonding of 3d metal (II) phthalocyanines with single-walled carbon nanotubes: a combined DFT and XPS study, Appl. Surf. Sci. 470 (2019) 622–630, https://doi.org/10.1016/j.apsusc.2018.11.159.
[72] M.S. Polyakov, T.V. Basova, M. Göksel, A. Şenocak, E. Demirbaş, M. Durmuş, B. Kadem, A. Hassan, Effect of covalent and non-covalent linking of zinc (II) phthalocyanine functionalised carbon nanomaterials on the sensor response to ammonia, Synth. Met. 227 (2017) 78–86, https://doi.org/10.1016/j.synthmet.2017.02.024.
[73] P. Krasnov, V. Ivanova, D. Klyamer, D. Bonegardt, A. Fedorov, T. Basova, Hybrid Materials Based on Carbon Nanotubes and Tetra-and Octa-Halogen-Substituted Zinc Phthalocyanines: Sensor Response Toward Ammonia from the Quantum-Chemical Point of View, Sensors 25 (1) (2024) 149, https://doi.org/10.3390/s25010149.
[74] F. Ahmed, M. Rashad, O. Saber, S. Kumar, A. Aljaafari, A. Ashoaibi, A.Z. Mahmoud, M. Ezzeldien, Low-temperature ethanol sensor via defective multiwalled carbon nanotubes, Materials 15 (13) (2022) 4439, https://doi.org/10.3390/ma15134439.
[75] L. Mahdavian, M. Monajjemi, N. Mangkorntong, Sensor response to alcohol and chemical mechanism of carbon nanotube gas sensors, Fuller. Nanotub. Carbon Nanostruct. 17 (5) (2009) 484–495, https://doi.org/10.1080/15363830903130044.
[76] V. Yılmaz, N. Can, A. Altındal, Adsorption of VOC vapors on ZnPc: sensing and kinetic studies, Environ. Sci. Pollut. Res. 31 (57) (2024) 65302–65314, https://doi.org/10.1007/s11356-024-35576-w.
[77] V. Yılmaz, N. Can, A. Altındal, Adsorption of VOC vapors on ZnPc: sensing and kinetic studies, Environ. Sci. Pollut. Res. 31 (57) (2024) 65302–65314, https://doi.org/10.1007/s11356-024-35576-w.
[78] G. Peng, E. Trock, H. Haick, Detecting simulated patterns of lung cancer biomarkers by random network of single-walled carbon nanotubes coated with nonpolymeric organic materials, Nano Lett. 8 (2008) 3631–3635, https://doi.org/10.1021/nl801577u.
[79] S. Freddi, M.C. Rodriguez Gonzalez, A. Casotto, L. Sangaletti, S. De Feyter, Machine-Learning-Aided NO_2 discrimination with an array of graphene chemiresistors covalently functionalized by diazonium chemistry, Chem. A Eur. J. 29 (60) (2023) e202302154, https://doi.org/10.1002/chem.202302154.
[80] V. Schroeder, S. Savagatrup, M. He, S. Lin, T.M. Swager, Carbon nanotube chemical sensors, Chem. Rev. 119 (1) (2018) 599–663, https://doi.org/10.1021/acs.chemrev.8b00340.
[81] D. Gounden, N. Nombona, W.E. Van Zyl, Recent advances in phthalocyanines for chemical sensor, non-linear optics (NLO) and energy storage applications, Coord. Chem. Rev. 420 (2020) 213359, https://doi.org/10.1016/j.ccr.2020.213359.
[82] H. Liu, Q. Li, B. Yan, L. Zhang, Y. Gu, Bionic electronic nose based on MOS sensors array and machine learning algorithms used for wine properties detection, Sensors 19 (1) (2018) 45, https://doi.org/10.3390/s19010045.
[83] S. Dhanekar, Smart and intelligent E-nose for sensitive and selective chemical sensing applications, Smart Sens. Environ. Med. Appl. (2020) 149–171, https://doi.org/10.1002/9781119587422.ch8.
[84] M. Aleixandre, J. Lozano, J. Gutiérrez, I. Sayago, M.J. Fernández, M.C. Horrillo, Portable e-nose to classify different kinds of wine, Sens. Actuators B Chem. 131 (1) (2008) 71–76, https://doi.org/10.1016/j.snb.2007.12.027.

Sonia Freddi is a Young Researcher at the *Institute of Photonics and Nanotechnology (IFN)* of the *National Research Council (CNR)*, working within the *LNESS laboratory* in Como, Italy. She graduated *cum laude* in Physics in 2016, at Università Cattolica (Italy), while she received *with distinction* the double PhD degree in Science (Università Cattolica-Italy) and Chemistry (KU Leuven-Belgium) in 2022. Her main expertise is related to the development of electronic noses, gas sensors, and 2D-material functionalization. Her research recently includes nanofabrication in a cleanroom environment, lithographies and solid-state dewetting for photonic applications. She has authored about 30 publications (including 21 as first author and 6 as corresponding) and holds an international patent. Her work has been recognized with numerous awards, including the Dario Nobili PhD Thesis Award, the Ermenegildo Zegna scholarship, and multiple Outstanding Reviewer Awards. She has delivered many oral presentations and invited talks and contributed to several conference and workshop organization. She is an active reviewer for many journals related to condensed matter physics and applied physics, she is guest editor for 2 special issues for *Materials* (MDPI), and since September 2025 she is a Young Editorial Board Member of *Nanomaterials* and *Sensors* (MDPI). She is currently coordinating as a PI the project BREATH-SENSE (2023–1506), supported by Fondazione Cariplo, and her project ANTIGONE (*Advanced e-Nose Technologies for Gas sensing of breath biomarkers to diagnOse and moNitor ongoing disEases*) has been recently awarded funding under the FIS3 Starting Grant call (grant n FIS-2024–02949). She has extensive teaching and mentoring experience at Università Cattolica and Politecnico di Milano, and she also spent effort in science outreach.

Monica Bollani is a Senior Researcher at the *Institute of Photonics and Nanotechnology (IFN)* of the *National Research Council (CNR)*, working within the *LNESS laboratory* in Como, Italy. She obtained a European Ph.D. in Materials Physics in 2000 from Marseille (France). Until 2004, she held a postdoctoral research position at ETH Zurich (Switzerland), focusing on SiGe epitaxial growth. She later joined IFN-CNR in Italy as a researcher, where her work initially concentrated on SiGe semiconductor growth and, since 2009, has expanded to include nano- and microfabrication. For more than ten years, she has led the semiconductor nanofabrication group (Group IV) at the LNESS laboratory, mainly dedicated to the nanostructuring of low-dimensional nanophotonic and nanoelectronic devices. She is currently the Principal Investigator of the Italian PRIN 2022 PNRR project ACONITE (*Food safety via microbial detection with photonic nanoresonators*, 2023–2025). In recent years, she coordinated the European project NARCISO (grant no. 828890), the CNR unit of the European Marie Curie project SONAR (grant no. 734690), as well as several other national projects. Dr. Bollani is co-chair of the international conference NANOSEA (most recent edition held in July 2024, Marseille). She has served on the organizing committees of several conferences, including the *8th ESPS-NIS 2010*, *FisMat 2013*, *MNE 2021*, and *ISTDM-ICSI 2023*. She has also been a member of the scientific advisory committees for *XTOP 2014*, *SPIE Photonics Europe 2022*, *D-Photon 2023*, *EOSAM 2024 and 2025*, and *E-MRS 2025*. Since October 2024, she has been serving as a Guest Editor for npj Nanophotonics (Nature journal). Previously, she was an Editor for Applied Optics (OPTICA, formerly OSA Journal) from December 2020 to November 2023, and Guest Editor for the special issue *"Multifunctional Coatings for Packaging Applications"* in the journal *Coatings* (MDPI).

Luigi Sangaletti is Full Professor of Condensed Matter Physics at the Università Cattolica del Sacro Cuore (UCSC). He graduated in Physics from the University of Milan in 1989 and, after being visiting scholar at the Department of Physics of Stanford University, obtained his Ph.D. from the University of Pavia in 1993, with a thesis on the electronic structure of strongly correlated oxides and fluorides. After postdoctoral work in the TERA-INFN collaboration and at GSI (Germany) on charged-particle beam cancer therapy, he joined UCSC in 1999, where he has since advanced through assistant, associate, and full professorships. His research focuses on the growth, characterization, and applications of nanostructured and low-dimensional materials, surface and interface physics, and light–matter interactions studied by advanced spectroscopic techniques such as XPS, UPS, ARPES, and XAS. His latest research focuses on developing electronic noses using an integrated approach that begins with the surface functionalization of sensing layers and extends to the design of innovative device architectures, spanning from chemiresistor arrays to virtual e-noses. He leads the Surface Science and Spectroscopy Laboratory (SSSL), promoting interdisciplinary research in materials physics at the Department of Mathematics and Physics of UCSC. Prof. Sangaletti has authored 200 + peer-reviewed scientific publications, has supervised 40 + graduate and doctoral students, and regularly contributes as referee for major journals in condensed matter and materials science.